Journal of Industrial and Engineering Chemistry 133 (2024) 577–587

Contents lists available at ScienceDirect

Journal of Industrial and Engineering Chemistry

journal homepage: www.elsevier.com/locate/jiec

Full Length Article

Zinc-rich polyester powder coatings with iron Phosphide: Lower zinc content and higher corrosion resistance

Jinbao Huang [a,b,d], Marshall Yang [b,c], Wenhao Zhu [b], Keyong Tang [e], Jian Chen [c], James Joseph Noël [c], Haiping Zhang [f], Liqin Wang [a,d,*], Hui Zhang [b,*], Jesse Zhu [b]

[a] School of Mechatronics Engineering, Harbin Institute of Technology, Harbin 150001, China
[b] Department of Chemical and Biochemical Engineering, Western University, London, ON, N6A 5B9, Canada
[c] Department of Chemistry, Western University, London N6A 5B7, Canada
[d] Zhengzhou Research Institute, Harbin Institute of Technology, Zhengzhou 450000, China
[e] School of Materials Science and Engineering, Zhengzhou University, Zhengzhou 450001, China
[f] Collaborative Innovation Center of Chemical Science and Engineering (Tianjin), School of Chemical Engineering and Technology, Tianjin University, Tianjin 300072, China

ARTICLE INFO

Keywords:
Iron phosphide
Zinc-rich
Powder coatings
Decreased zinc content
Corrosion acceleration

ABSTRACT

Many conductive fillers such as carbon black, carbon nanotube and graphene, have been developed to reduce zinc content for zinc-rich coatings, but very few of them could reduce zinc content by 10 % while maintaining the original corrosion protection ability. The carbon-based conductive additives have the issue of corrosion promotion after cathodic protection. In this study, low-cost iron based conductive additive, iron phosphide was used to reduce zinc content in environmentally friendly zinc-rich polyester powder coatings. We investigated the anticorrosive performance of the prepared coatings by open circuit potential, electrochemical impedance spectroscopy measurements and neutral salt spray tests. The corrosion products were analyzed with Raman spectroscopy, X-ray diffraction and scanning electron microscopy equipped with energy dispersive X-ray spectroscopy. It was found that iron phosphide, due to its conductive nature, inert chemistry, activation function and barrier effect of the lamellar shape, can establish cathodic protection at a low zinc content of 45 wt% with an active protection period of 20 days. It can replace 10 wt% of zinc in 75 wt% zinc-rich polyester powder coatings while maintaining the original cathodic protection ability, as long as 86 days for a 40 μm film. In addition, iron phosphide can significantly inhibit localized corrosion and decrease corrosion creepage by about 20 % during 2500 h salt spray tests. Moreover, a possible corrosion protection mechanism for iron phosphide in zinc-rich polyester coatings was proposed.

Introduction

Zinc-rich coatings have been extensively used in industrial anticorrosive practice for decades [1,2]. They are suitable for steel rust prevention in automotive industry and marine environment. In zinc-rich coatings, electrochemically more active zinc particles sacrifice themselves to provide cathodic protection for the steel substrate [3]. The performance of zinc-rich coatings is mainly determined by the flow of galvanic current from the zinc particles to the oxygen adjacent to the substrate [2]. In case that there is sufficient electrical connection between the zinc particles and the substrate, the metallic substrate is galvanically protected. Usually, higher zinc content results in longer cathodic protection [4]. Hence, the zinc content in zinc-rich coatings is usually very high, ranging from approximately 65 wt% to 93 wt% of the dry film [5]. When the cathodic protection fails, the zinc-rich coatings still protect the substrate with a reinforced barrier effect resulting from the formation of zinc corrosion products [3,6].

However, high zinc content in paints leads to high cost, difficulty in rheology and leveling during curing, as well as problems in paint storage [4]. The zinc oxide smoke released during welding and cutting is directly related to “zinc fever” among factory operators [7,8]. In addition, as only about 30 % of zinc is consumed working as sacrificial anode when cathodic protection expires [9,10], many efforts have been made to reduce zinc content while maintaining the pristine cathodic protection

* Corresponding authors at: School of Mechatronics Engineering, Harbin Institute of Technology, Harbin 150001, China (Liqin Wang); Department of Chemical and Biochemical Engineering, Western University, London, ON N6A 5B9, Canada (Hui Zhang).
E-mail addresses: lqwang@hit.edu.cn (L. Wang), hzhang1@uwo.ca (H. Zhang).

https://doi.org/10.1016/j.jiec.2023.12.035
Received 10 July 2023; Received in revised form 3 November 2023; Accepted 13 December 2023
Available online 15 December 2023

of the coatings. Two strategies have been proposed. One is to incorporate electrical connectors to make better use of the zinc. These additives include iron phosphide [11–14], aluminum pigments [15], carbon black [16,17], graphene [18–20], carbon nanotube [21], carbon fiber [22], ZnS@C core–shell nanosphere [23], stainless steel flake [24], conductive lamellar mica [25], zinc fiber [26], nanoparticulate zinc [27,28], lamellar zinc flakes [1,29], polypyrrole and polyaniline [30,31], and 2D transition metal carbide/nitride material (MXene) [32].

The other is to add barrier additives to slow down the ionic diffusion of aggressive species. Such additives can be like micaceous iron oxide [15], and nano-montmorillonite [33], graphene oxide and its composite [34]. However, carbon-based conductive additives such as carbon black, carbon nanotube, graphene and MXene have been reported to aggravate localized corrosion at exposed metal-coating interfaces and accelerate corrosion of iron after cathodic protection [35–38]. In addition, very few additives were able to replace more than 10 wt% of zinc particles while maintaining the original cathodic protection performance. Considering the high zinc content in zinc-rich coatings and increasing demand for high quality zinc-rich coatings, more effective additives with no corrosion promotion effects should be explored for zinc-rich coatings.

Among the reported additives for zinc content reduction, iron phosphide, the byproducts of phosphorus mining, was proven a cost-efficient conductive extender. 12 wt% of iron phosphide decreased the zinc content from 84 to 77 wt% with minimal (about 25 %) decrease in cathodic protection in ethyl silicate zinc-rich coatings. But in epoxy-polyamide coatings, iron phosphide caused more than 90 % loss of the original cathodic protection ability [11–14,39]. It seems that iron phosphide has independence with coating systems. As for the corrosion protection mechanisms of iron phosphide for replacing zinc, researchers have different opinions. Feliu S. et al. [12] believe that di-iron phosphide work as conductive extender and increase coating film compactness. But a recent study [40] revealed that di-iron phosphide can promote zinc activation but also high porosity, and high amount (such as 12 %) of di-iron phosphide would reduce cathodic protection ability. It is also worth mentioning that all the studies above were based on liquid coatings. Powder coatings involve no harmful volatile organic compounds (VOCs), are increasingly taking over the market of liquid coatings. Zinc-rich coatings based on powder coatings demonstrate denser coating structure, better protection than and different protection mechanisms with the liquid-based coatings on a same zinc content [2,16,41,42]. However, there is no report on the utilization of iron phosphide in environmentally friendly powder coatings. This would prevent the development of zinc-rich powder coatings of low cost and high performance for environmentally-friendly applications.

Herein, iron phosphide was incorporated into a zinc-rich powder coating. Polyester (PE) /triglycidyl isocyanurate (TGIC) was selected as the base binder (the combination of coating resin and curing agent) for its acceptable substrate adhesion and good outdoor durability. These two characters enable polyester-based zinc-rich coatings to work as a single-layer coating and double-layer coatings as both the primer and topcoat for outdoor applications. The single-layer polyester-based zinc-rich coatings with high corrosion resistance and outdoor durability can be used for general purposes, while the double-layer zinc-rich coatings can be used for heavy duty outdoor applications. The anti-corrosive performances of the fabricated coatings were characterized by open circuit potential (OCP), neutral salt spray tests and electrochemical impedance spectroscopy (EIS), and the corrosion products were also analyzed. This work not only presents a unique zinc-rich coating with low zinc content and high protection performance, but also provides a mechanistic insight into the corrosion protection of steel with zinc particles and non-carbon based conductive additive such as iron phosphide.

Experimental

Materials

PE/TGIC clear powder coating procured from TCI Powder Coatings (USA) was used as the base binder. Zinc dust (mean particle size of approximately 7 μm, 7.1 g/cm^3) purchased from North Zinc Dust (Canada) worked as the sacrificial anode in zinc-rich coatings. Iron phosphide powder (about 6.9 g/cm^3) from Anhui Sihuan Painting Co., Ltd. (China) was employed to replace part of zinc particles. Standard Q-panel steel panels were purchased from Q-Lab Corporation (USA).

Preparation of coating powders and coated panels

Fabrication process of the zinc-rich PE powder coatings containing iron phosphide is illustrated in Fig. 1. All the components (Table 1) were thoroughly pre-mixed with a high-speed blender, extruded with a twin-screw extruder (SLJ-10, Yantai Donghui Powder Processing Equipment Co., Ltd., China) at screw speed of 300 rpm and an extrusion temperature of 100 ℃. The obtained chips were pulverized and sieved to coating powders with a median particle size of about 40 μm. These powders were then sprayed onto standard Q-panel steel panels with an electrostatic spraying gun (ITW Gema, Switzerland) in a powder coating spray booth (N902, Nordson Corporation, USA) at –70 kV and 15 cm away from substrate. Finally, the deposited coating powder was cured at 200 °C for 15 min. The thickness of the obtained coating films was 40 ± 4 μm as measured by a thickness gauge (PosiTector 6000, DeFelsko Corporation, USA).

Characterization of iron phosphide and coating films

The chemical composition of iron phosphide powder was analyzed using X-ray diffraction (XRD, Smartlab, Japan) and a scanning electron microscope equipped with energy dispersive X-ray spectroscopy (SEM/EDS, SU3900, Hitachi, Japan) at an accelerating voltage of 15 kV. The coated panels were sectioned, mounted into epoxy, polished, and sputtered with gold for observation of the cross-sectional morphology by SEM/EDS under 15 kV.

Neutral salt spray and electrochemical tests

The corrosion performances of the zinc-rich PE coatings containing iron phosphide was evaluated by neutral salt spray test and electrochemical impedance spectroscopy (EIS). Neutral salt spray tests were conducted as per ASTM B117–16 in a salt spray chamber (MX-9204, Associated Environmental Systems, USA). Two 0.5 mm intersecting scribes were made on the coating panels prior to tests. These tests were conducted for 2500 h for three parallel coating panels. The corrosion creepage was acquired by measuring the average scribe width after the tests with two parallel straight lines. EIS measurements were carried out on a Solartron Modulab XM MTS (AMETEK Inc., USA) electrochemical workstation with 3.5 wt% NaCl solution in a three-electrode system. A saturated calomel electrode (SCE) worked as reference electrode, a platinum foil was used as the counter electrode, and the coated panels with exposed areas of 20.25 cm^2 were the working electrodes. The measurements were conducted from 10^5 Hz to 0.01 Hz with a sinusoidal voltage amplitude of 10 mV. At least two visually defects free coating panels with a total of at least three exposed areas either at the top, middle or the bottom of the coating panel were used for electrochemical tests. During the first week, OCP and EIS were conducted on every exposed area until consistent results were obtained, and a representative area was selected for the later electrochemical tests.

Corrosion products analysis

The corrosion products formed in the scribed regions on steel

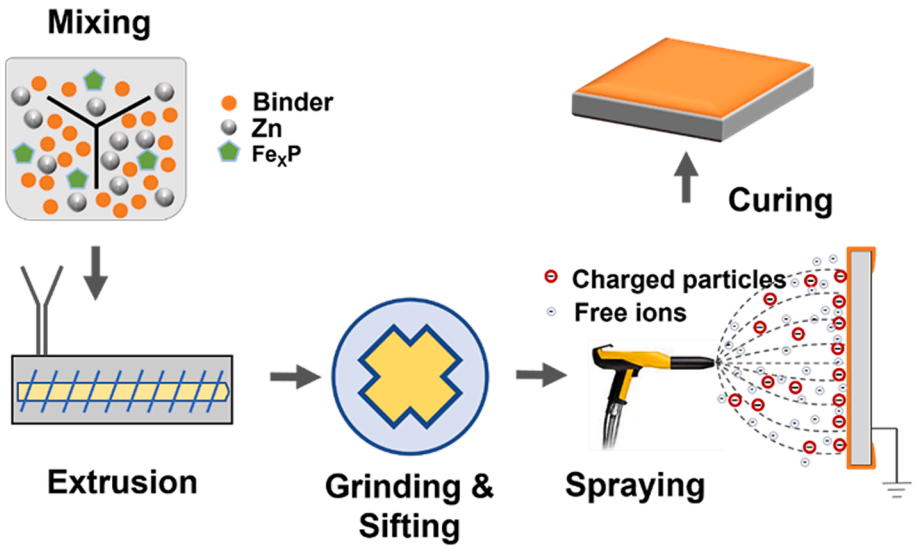

Fig. 1. Schematic for the fabrication process of powder coatings containing iron phosphide.

Table 1
Naming of the prepared zinc-rich coatings with different contents of iron phosphide.

Sample name	Binder / g	Zinc dust / g	Iron phosphide / g
Zn75	25	75	0
Zn65P10	25	65	10
Zn55P20	25	55	20
Zn45P30	25	45	30

substrates were characterized using Raman microscope (Model 2000, Renishaw, UK) and XRD. Elemental compositions of the corrosion products in and near the scribed areas were analyzed using SEM/EDS under 10 kV. The scanning areas for elemental composition analyses were about 2 mm long along the scribe and 0.5 mm wide perpendicular to the scribe. EDS measurements were repeated 3 times for obtaining an average elemental ratio. The morphology and composition of corrosion products on steel substrates after EIS tests were characterized with SEM/EDS and confocal laser scanning microscopy (CLSM 900, Carl Zeiss Microscopy GmbH, Germany). The obtained CLSM data were processed with ConfoMap version 7.4.8341 to acquire 3D topographical images and surface roughness values. The optical images were taken by an optical microscope (OM, VHX-950F, Keyence Corporation, Japan).

Results and discussion

Iron phosphide powder morphology and distribution in coating film

Fig. 2 shows the morphology and chemical composition of the iron phosphide powder. These iron phosphide particles were in sizes ranging from approximately 1 to 25 μm (Fig. 2a), with considerable amount of laminar shaped Fe_xP, as marked by the orange rectangles. As confirmed by EDS and XRD, iron and phosphorous are the main elements (Fig. S1), and the main components included iron phosphide (FeP), di-iron phosphide (Fe_2P) and magnetite (Fe_3O_4) (Fig. 2b). The major peaks at 48, 33, 47, 46 and 37° were attributed to FeP. The peaks at 40, 44, 47° to Fe_2P, and the peaks at 35 and 62° to Fe_3O_4, respectively. Both FeP and Fe_2P were electrically conductive to function as zinc particle connectors [11–14], and the iron phosphide powder was referred as Fe_xP.

Due to its conductive nature, Fe_xP can electrically connect zinc particles in zinc-rich coating films [11–14]. However, to achieve this goal, Fe_xP should be well distributed among the zinc particles. The cross-

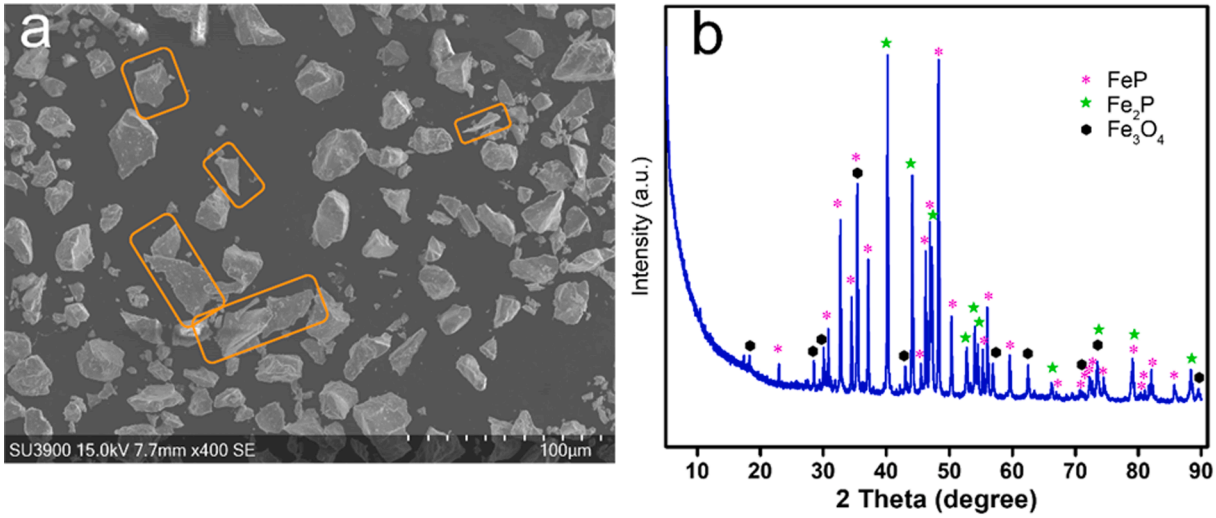

Fig. 2. (a) SEM image and (b) XRD spectrum of iron phosphide powder. (Orange rectangles indicate laminar shape Fe_xP). (For interpretation of the references to color in this figure legend, the reader is referred to the web version of this article.)

sectional morphologies of the zinc-rich coatings containing Fe_xP are shown in Fig. 3. The irregular Fe_xP particles with larger aspect ratio than the zinc particles exhibited close contact and had some point-to-point connections with these zinc particles. It was noted that Fe_xP particles had different iron to phosphorous ratios (Fig. 3e), corresponding to the existence of Fe_2P and FeP in the Fe_xP powder.

Electrochemical measurement results

The electrochemical performance of zinc-rich coating containing Fe_xP were analyzed by open circuit potential (OCP) and EIS measurements under natural corrosion conditions. OCP allows analysis of the electrochemical activity of a steel substrate coated with a zinc-rich coating film. An OCP value below –0.78 V/SCE indicates that the steel is cathodically protected [43]. EIS is effective in offering insights into how organic coating films degrade with the electrolyte ingress [44–46]. In addition, a higher pore resistance (R_{pore}) obtained through data fitting with electrical equivalent circuits (EECs) indicates better barrier effect for a coated panel [44,47,48].

Fig. 4 shows the variations of OCP, pore resistance, EIS Bode frequency-modulus and Bode frequency-phase angle plots and Nyquist plots for the zinc-rich coatings containing Fe_xP in 3.5 wt% NaCl solution with immersion time (t). The corrosion processes of these coated panels could be generally divided into three stages as seen from Fig. 4a. The first stage (fluctuation) was $0 < t < 11$ days when the OCP value underwent a rapid increase and decrease, and the pore resistance values (Fig. 4b) decreased to the lowest of approximately 10 $k\Omega \cdot cm^2$. At the same time, the impedance at low frequency region (10^{-2}-10^{0} Hz) in bode modulus plots rapidly decreased. The phase angle at high frequency region (10^{3}-10^{5} Hz) turned more positive. And the semicircle in the Nyquist plots quickly diminished, demonstrating the degradation of coating barrier properties. This stage was related to the ingress of electrolyte and accumulation of zinc corrosion products in the coating films and on the surface [49]. In the experiments, white corrosion products were visible on the coating films after 5 days of immersion, which could temporarily cut off the electrical connections between the zinc particles and steel [50]. With the gradual ingress of electrolyte, the zinc particles were reconnected with the steel [49].

During the second stage (the starting and terminal time varied for different samples, e.g., $11 < t < 86$ days for Zn75), the OCP value generally remained below the red dashed line (–0.78 V/SCE) and the R_{pore} varied and slightly increased. The impedance at low frequency region gradually recovered and increased. The phase angle at high frequency region went into more negative region. The Nyquist plots also showed larger semicircles as immersion went on. This was the stage when the steel substrate was in cathodic protection. As the immersion extended, when more zinc corrosion products accumulated inside the pores and channels, and the remaining zinc particles could not provide sufficient electrical connections with the steel, the third stage started (i.e., $t > 86$ days). The OCP shifted to more positive region (>–0.78 V/SCE) and the pore resistance kept rising at this stage. The barrier effects of these zinc-rich coating films began to dominate in the corrosion protection action.

Since the coated panels were free from corrosion during the first and second stages, the total time frame of the first two stages was regarded as the overall active protection period (APP). As shown in Fig. 4 and Table 2, Zn75 exhibited 75 days of cathodic protection and 86 days of APP, and Zn65P10 showed similar cathodic protection period (77 days) and APP (84 days), demonstrating the superior connecting performance of Fe_xP particles among Zn particles in polyester powder coatings. It should be noted that such a long cathodic protection period is more advantageous than many reported zinc rich coatings with conductive additives as shown in Table 3. The Zn65P10 zinc rich polyester powder coatings reached reduction of zinc content from 75 % by 10 % with equivalent weight of Fe_xP. The powder based Zn65P10 with a low film thickness of 40 μm, demonstrated much longer cathodic protection period than liquid based zinc rich coatings with more than 80 % zinc, and zinc rich coatings with graphene, Fe_2P and stainless-steel flakes. Considering the low cost of Fe_xP powder as mining byproduct, the material cost of zinc rich coatings could be cut down by about 10 % with Fe_xP. More importantly, Fe_xP has no risk of corrosion promotion after cathodic protection. All these findings prove Fe_xP is an effective conductive additive for zinc rich polyester powder coatings.

Zn55P20 showed about 20 % decrease in APP (69 days) as compared with that of Zn75. The 40 μm Zn45P30 coating film realized cathodic protection for the substrate at a zinc content as low as 45 wt% and demonstrated an APP of about 20 days, even longer than an 80 μm epoxy powder coating film with 40 wt% zinc particles and 10 wt% zinc flakes (18 days) [16]. In prior studies about iron phosphide, inclusion of Fe_2P was accompanied with significant reduction of APP [11,12]. In ethyl silicate zinc-rich coatings, replacing 7 wt% zinc from 84 wt% with 12 wt % Fe_2P decreased about 25 % of the original APP, while replacing 25 wt % zinc from 84 wt% with equivalent weight of Fe_2P decreased about 50 % of the original APP, not to mention the epoxy-polyamide system where replacing 11 wt% zinc in 97 wt% zinc with equivalent weight of Fe_2P reduced more than 90 % of the original APP [12]. All these findings indicated that Fe_xP presents superior advantages in polyester powder coatings to connect zinc particles and decrease zinc content while maintaining the original cathodic protection.

As Zn65P10 demonstrated the longest APP among the Fe_xP containing coating panels, EIS together with fitting were used to analyze their performances under immersion. Their EIS Bode-modulus, Bode-

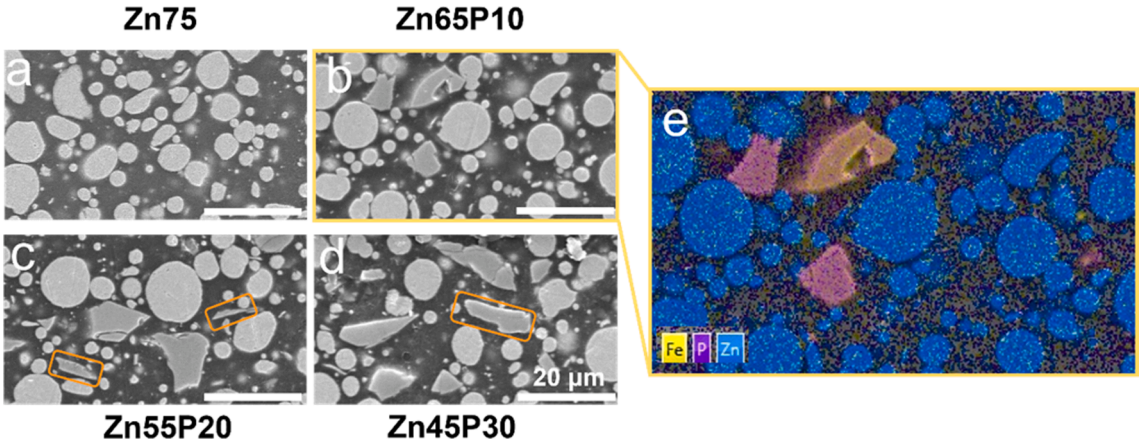

Fig. 3. Cross-sectional SEM images of (a) Zn75, (b) Zn65P10, (c) Zn55P20 and (d) Zn45P30; (e) EDS mapping image of Zn65P10 (Orange rectangles indicate lamellar shaped Fe_xP). Scale bar 20 μm. (For interpretation of the references to color in this figure legend, the reader is referred to the web version of this article.)

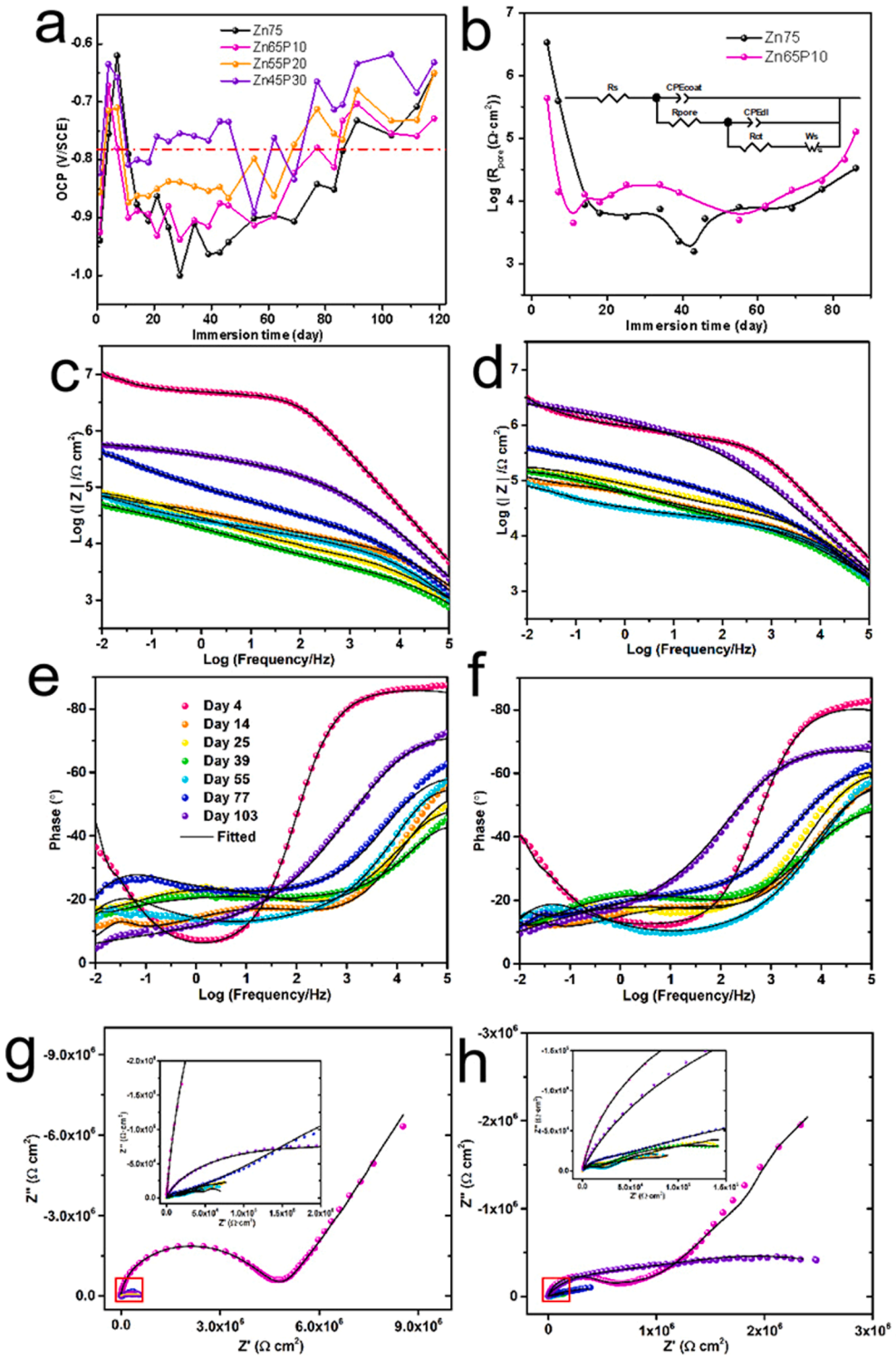

Fig. 4. (a) OCP, (b) pore resistance (R_{pore}), (c-d) EIS Bode plots, (e-f) phase plots and (g-h) Nyquist plots for the iron phosphide containing zinc-rich coatings during 103 days of immersion in 3.5 wt% NaCl solution. Zn75 (c, e and g), Zn65P10 (d, f and h). Below the red dash line in (a) is cathodic protection region. The inset in (b) is the equivalent electrical circuit for fitting. The insets in (g) and (h) are the magnified figures of the corresponding red circle regions. The fitted spectra were also shown as the black connected lines. (For interpretation of the references to color in this figure legend, the reader is referred to the web version of this article.)

phase plots and Nyquist plots are shown in Fig. 4c–f. The EIS spectra were fitted with the most used equivalent electrical circuit (EEC) model as shown in the inset of Fig. 4b for coating film with defects. During fitting, constant phase elements (CPEs) and double layer were utilized to replace pure capacitors due to the intrinsic inhomogeneity of the coating film and the interfaces [47,48]. Proper fittings results were obtained as shown by the χ^2 lower than 10^{-4} as shown in Table S1 and S2 and the overlapping between the measured and fitted spectra in Fig. 4. CPEcoat is directly related to the capacitance of the coating film and it is reversely related to coating pore resistance (R_{pore}). CPE_{dl} and R_{ct} are double-layer constant phase and charge-transfer resistance, respectively, relating to the interface reaction between the coating film and

Table 2
The duration of the first two stages and the total active protection period (APP) for coatings with different contents of iron phosphide during electrochemical testing when immersed in 3.5% NaCl solution.

Sample name	1st stage / Day	2nd stage / Day	APP / Day
Zn75	11	75	86
Zn65P10	7	77	84
Zn55P20	9	60	69
Zn45P30	11	9	20

substrate and R_{ct} is inversely proportional to the corrosion rate of the sample. A Warburg element with short circuit terminus W_s was used to corelate the straight line in the Nyquist plot, indicating the diffusion of oxygen and zinc corrosion products.

The results show that during the first stage, Zn65P10 demonstrated lower impedance at 0.01 Hz (6.5×10^6MΩ·cm^2), less negative phase angle (-83°) and smaller semicircle in Nyquist plots than did the Zn75 (1.0×10^7 Ω·cm^2, −89°). The R_{pore} for Zn65P10 (4.37×10^5 Ω cm^2) was about one order of magnitude smaller than that for Zn75 (3.37×10^6 Ω cm^2). The resistance component of Ws (8.27×10^6 Ω·cm^2) was about half order of magnitude smaller than that for Zn75 (2.37×10^7 Ω cm^2). Such low resistance against electrolyte ingress would lead to rapid corrosion of zinc particles and accumulation of zinc corrosion products inside the coating channels and pores.

After about 14 days of immersion, the impedance and phase angle for Zn65P10 quickly exceeded those for Zn75 during this second stage. Meanwhile, the R_{pore} for Zn65P10 (1.27×10^4 Ω cm^2) exceeded that for Zn75 (8.71×10^3 Ω cm^2), although both had dramatic decline. This leading superiority remained as immersion went on after about 14 days. And the R_{pore} gradually increased with the accumulation of corrosion products. This larger R_{pore} represents higher shielding effect against the corrosive species such as Cl^-, H_2O and O_2 penetrating the coating film. This trend also corresponds to the lower CPE_{coat} value of Zn65P10 than that of Zn75 at later stage of immersion. The value of R_{ct} for the Zn65P10 was about octant to one order of magnitude larger than that for the Zn75 after 14 days of immersion. This higher R_{ct} value indicates sluggish charge transfer reaction, corresponding to the inhibited ionic connectivity between the zinc particles and the substrate via the electrolyte and low rate of corrosion inside Zn65P10. This is in line with the change of Warburg that more zinc corrosion products formed inside Zn65P10 coating than inside Zn75.

When all the zinc-rich coating films failed to provide cathodic protection (86 days), the corrosion products on the coating film surface were characterized with XRD (Fig. S2). Zn75 and Zn65P10 showed similar composition in corrosion products. $Zn_5(OH)_8Cl_2{\cdot}H_2O$ was the dominant corrosion product [52], while $Zn_4CO_3(OH)_6{\cdot}H_2O$ also formed due to the reaction of the metal hydroxide with the dissolved CO_2. The minor XRD peaks for zinc revealed that zinc was not fully consumed even near the coating film surface after cathodic protection in zinc-rich powder coatings. The coating films were stripped off to analyze the corrosion products underneath the coating films. It was found that the substrates displayed many white spots (Fig. 5a–d) smaller than 1 mm in diameter and about 30 μm in height over the substrate at the end of the APP (Fig. 5e). The number of white spots became fewer with the increase of Fe_xP content in the coating film. The substrate under the Zn75 coating film showed the highest counts of the white spots, while that under Zn45P30 presented no visible ones. The chemical components of the white spots were analyzed with SEM/EDS. As shown in Fig. 5f, the white spots consisted of zinc, chloride, and oxygen, but were iron depleted. These chemical components and the white color indicated that they were zinc corrosion products usually found at porous areas in coating films and substrate interfaces [52]. The fewer zinc corrosion products underneath Fe_xP containing coating films demonstrated that Fe_xP containing zinc-rich coating film had better barrier effects [11] and kept substrates free from corrosion even after cathodic protection when immersed in 3.5 wt% NaCl solution.

Neutral salt spray results

Neutral salt spray test, a widely accepted method in coating industry, was also utilized to evaluate the protection performance of coating films against corrosion. A narrower creepage indicates better protection for the steel substrate. The surface images of zinc-rich coating panels after neutral salt spray tests elapsed for 1000 h, 2000 h and 2500 h are presented in Fig. S3, and Fig. 6. The Zn75 and Zn65P10 demonstrated similar corrosion creepages on the scribes throughout the neutral salt spray tests. However, unlike Zn75 showing several visible localized corrosion sites as indicated by the red arrows in Fig. 6a, all the other coating panels exhibited very few localized corrosion sites, indicating that coating films with Fe_xP had higher localized corrosion resistance than Zn75. As zinc occupies the majority of the coating material cost, a reduction of 10 % zinc with the cost-effective Fe_xP in 75 % zinc-rich coatings could decrease about 13 % of the material cost.

To analyze the corrosion products of Fe_xP containing zinc-rich coating panels, the coating films were stripped off (Fig. S4) using paint stripper, which removed the organic zinc-rich coating films and the embedded zinc particles but left the inorganic corrosion products. The corrosion products along scribes were analyzed with OM, XRD, Raman and SEM, respectively. The substrate coated with the Zn75 coating film exhibited more localized corrosion sites than those underneath Fe_xP containing coating films, and most of the Zn75 corrosion sites were off the scribes. It is known that zinc-rich coatings could inhibit localized corrosion to some extent, but these phenomena indicate that cathodic protection by zinc-rich coating cannot eliminate localized

Table 3
Coating characters and cathodic protection periods of zinc rich coatings in the literature.

Binder	Zinc content wt. %	Conductive additive	Dry film thickness /μm	Cathodic protection period /d	Corrosion promotion risk	Reference
Epoxy	90	0.25 % Graphene	65	25	Yes	[19]
Epoxy	70	0.5 % Graphene	100	25	Yes	[51]
Epoxy	85	N/A	100	70	N/A	[24]
Epoxy	80	2.5 % Stainless steel flakes	100	70	No	[24]
Epoxy	75	5 % Stainless steel flakes	100	40	No	[24]
Ethyl silicate	84	N/A	60	80	N/A	[12]
Ethyl silicate	84	12 % Fe_2P	60	78	No	[12]
Ethyl silicate	77	12 % Fe_2P	60	60	No	[12]
Epoxy	78	6 % Fe_2P & 0.5 % silane	65	19	No	[40]
Epoxy powder coating	40	10 % Zinc flake & 2.1 % PANI-Cl	70	90	No	[31]
Polyester powder coating	75	N/A	40	86	N/A	This work
Polyester powder coating	65	10 % Fe_xP	40	84	No	This work

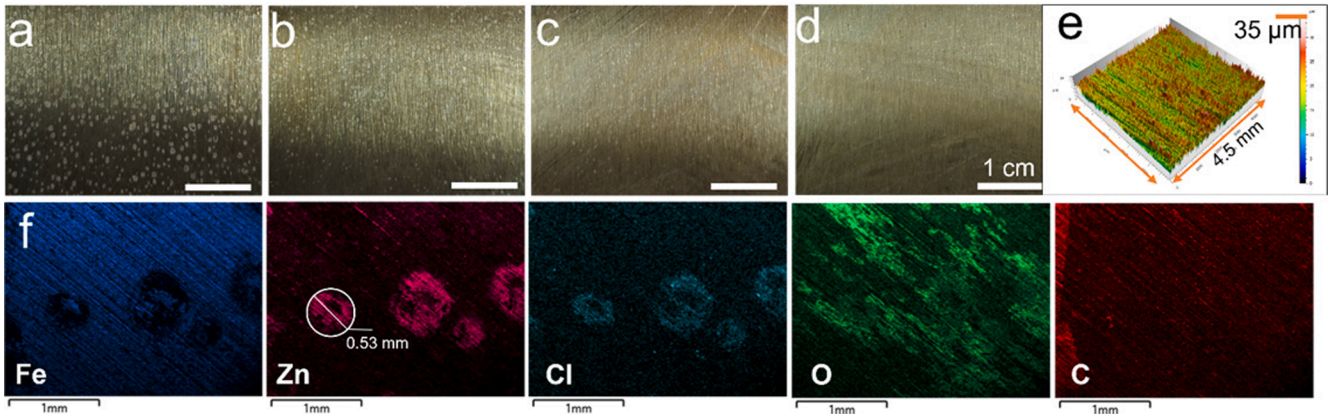

Fig. 5. Optical images of the substrates under (a) Zn75, (b) Zn65P10, (c) Zn55P20, (d) Zn45P30 zinc rich coating films when cathodic protection failed (after about 86 days of immersion). The scale bar is 1 cm. (e) 3D CLSM image of a white spot on Zn75. (f) EDS mapping images on Fe, Zn, Cl, O and C element for the white spots on Zn75. The scale bar is 1 mm.

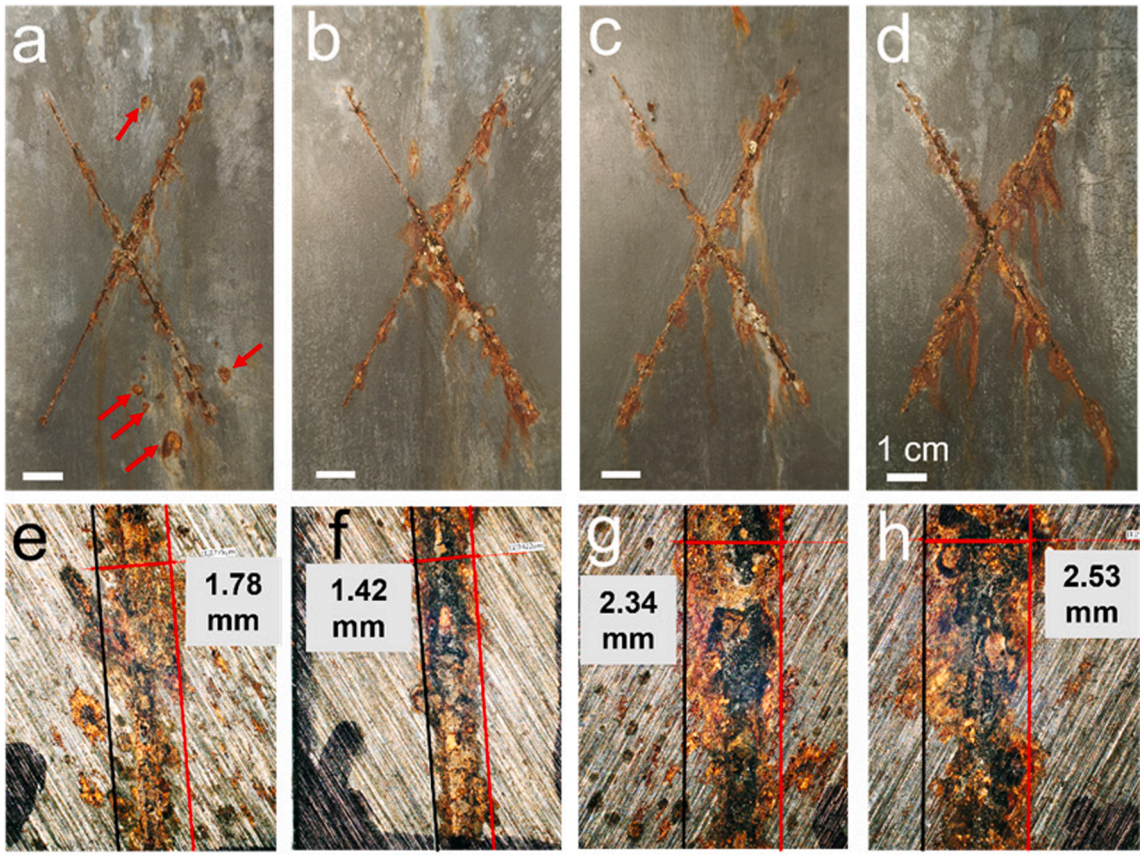

Fig. 6. Optical photos of (a) Zn75, (b) Zn65P10, (c) Zn55P20 and (d) Zn45P30 after 2500 h of neutral salt spray exposure at 37 °C with 5 % NaCl concentration. The scale bar is 1 cm. Optical images of (e–h) the corresponding corrosion creepage on each substrate. The distance between the red line and black line represents the average creepage. The red arrows indicate localized corrosion. (For interpretation of the references to color in this figure legend, the reader is referred to the web version of this article.)

corrosion. The substrate underneath the Zn65P10 coating film exhibited the least local corrosion sites, and the narrowest corrosion creepage (1.43 mm) than those for Zn75 coating film (1.78 mm), Zn55P20 coating film (2.34 mm) and Zn45P30 coating film (2.53 mm), as shown in Fig. 6e–h. It is suggested that the Zn65P10 coating film provided the best corrosion protection among the tested samples during the neutral salt spray tests. The phenomenon indicates that Fe_xP containing zinc-rich coatings could provide better localized corrosion inhibition ability than pure zinc-rich coatings.

The corrosion products along the scribes were observed as micro-particles with different colors, including yellow, orange, red, brown and black (Fig. 6e and h), which were common corrosion products of steel in aerobic environments [53–56]. The XRD results in Fig. 7a show that Zn75 and Zn65P10 demonstrated similar corrosion products such as goethite (α-FeOOH), akageneite (β-FeOOH) as well as magnetite (Fe_3O_4). However, Zn65P10 showed much stronger peaks for Fe_3O_4 and weaker peaks for iron than Zn75, indicating the dense structure and strong shielding of Fe_3O_4 on the scribed areas. Raman characterizations

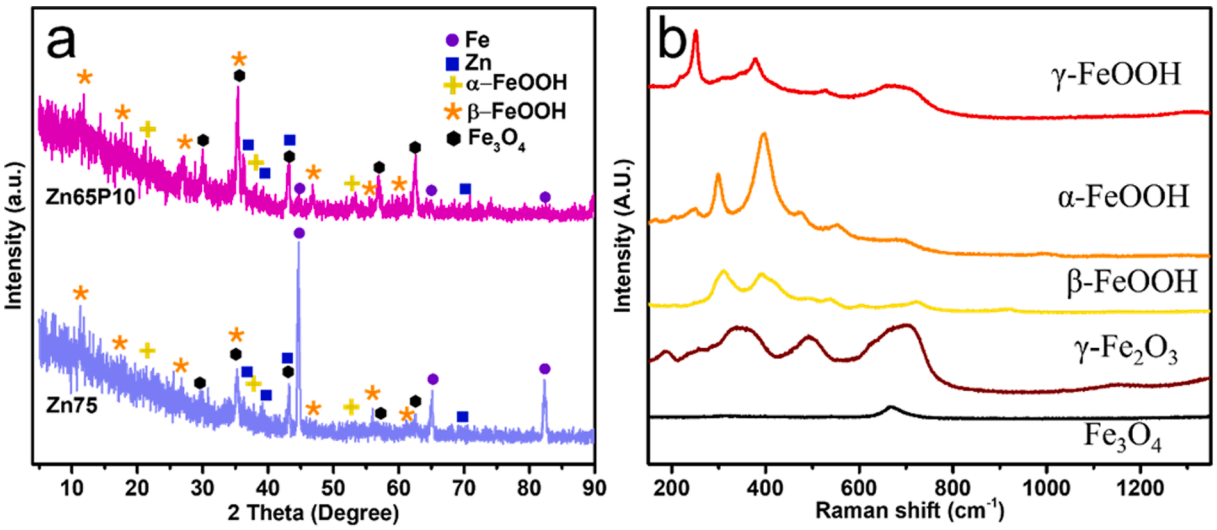

Fig. 7. (a) XRD pattern and (b) Raman spectra of the corrosion products along the scribed regions of Zn75 and Zn65P10.

proved that the items with light colors, including yellow, orange and red, were α-FeOOH, β-FeOOH and γ-FeOOH, respectively [53,55]. Those with dark colors (i.e., brown and black) were γ-Fe_2O_3 and Fe_3O_4, respectively [41], corresponding to the curves with the same color in Fig. 7b. It should be noted that the substrates beneath the Fe_xP containing coating films showed more black corrosion products, which means more Fe_3O_4 formed in the scribed areas of those Fe_xP containing coating panels. In addition, the corresponding elemental ratios of the corrosion products along the scribes (Fig. 8) showed that corrosion products beneath Fe_xP containing coating films were more O_2 depleted than those beneath Zn75 coating film. The corrosion products beneath Zn75 demonstrated the lowest iron to oxygen ratio (0.84: 1, calculated from the EDS analyses of the insert in Fig. 8.), lower than that of rusts beneath Zn65P10 (0.91: 1), Zn55P20 (0.99: 1) and Zn45P30 (0.97:1). The higher iron to oxygen ratios of the corrosion products also confirmed that the coatings with Fe_xP had strong barrier effects to inhibit the diffusion of corrosive species such as O_2.

Corrosion protection mechanisms

The improved corrosion resistance of zinc-rich coating films at a decreased zinc content took place due to four reasons. The first reason is

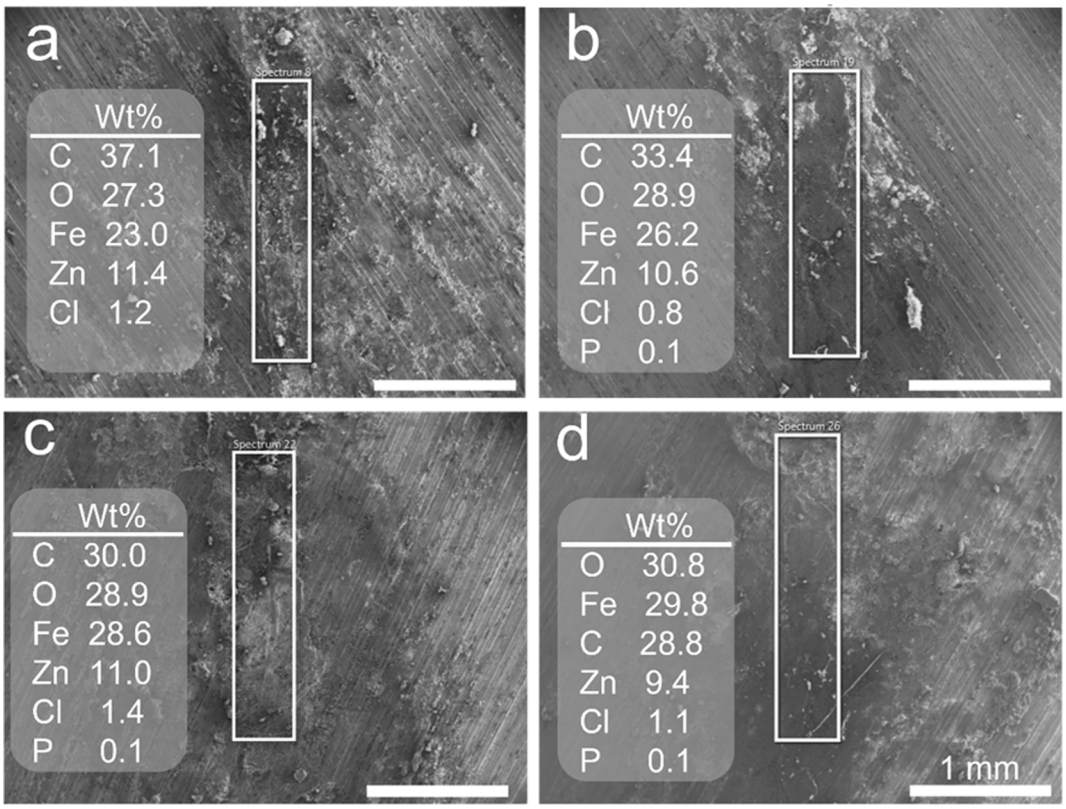

Fig. 8. SEM images of substrates beneath (a) Zn75, (b) Zn65P10, (c) Zn55P20 and (d) Zn45P30. The insets were the elemental ratios for the selected regions along the scribes. At least 3 areas were measured to obtain an average value under 10 kV accelerating voltage.

the electrical connectivity of the near spherical and lamellar Fe_xP, which enabled zinc particles to be electrically connected with each other and with the substrate and form effective electron conduction network. This can be confirmed by the establishment of cathodic protection at a low zinc concentration of 45 wt% (Fig. 3). The second is the inert chemistry of FeP and Fe_2P, which protected them free from corrosion and reduced the risk of electrical connection failures that could be caused by corrosion of zinc particles. The third is the barrier effect of the lamellar Fe_xP [11,40], which elongated the diffusion pathways of corrosive species (e.g., O_2, water and Cl^-) going through the coating films [31,43]. The forth one is the slightly high porosity and the activation function of Fe_xP. The former enabled rapid ingress of electrolyte, while the later activated zinc particles to corrode and formed more zinc corrosion products. This phenomenon could be translated to a high utilization of zinc. The blocked channels at the first stage would lead to the high barrier and low corrosive species penetrating the coating at the second stage. Then there would be regions with less O_2 along the interfaces of coating film and substrate and production of low O/Fe ratio corrosion products (Fig. 8). In addition, Fe_xP as an iron-based alloy, has no corrosion-accelerating effect after the cathodic protection, unlike carbon based electrical connectors such as graphene [53,57], carbon nanotube [58] and carbon black [10]. As a result, even when the cathodic protection was failed, the coating film corrosion was still dominated by the barrier effect. The Zn65P10 demonstrated a high impedance modulus of 6.4 MΩ cm^2 at the 0.01 Hz after 103 days of immersion.

We propose plausible corrosion protection mechanisms for the zinc-rich PE coatings with and without Fe_xP. For zinc-rich coatings without Fe_xP (Fig. 9a), with the ingress of aggressive species (O_2, H_2O and Cl^-), the zinc particles electrically connected to the steel substrate worked as sacrificial anode to protect steel, leading to the oxidation of Zn into Zn^{2+}. The electrons generated by Zn oxidation transferred to the cathodic region where O_2 was reduced to OH^-, and the dissolved Zn^{2+} would hydrolyze, react with chloride or the dissolved CO_2 in the pores, and form corrosion products (i.e., $Zn_5(OH)_8Cl_2$ and $Zn_2CO_3(OH)_2$, Fig. S2). With the gradual dissolution of zinc particles and the accumulation of zinc corrosion products, zinc particles could not provide sufficient galvanic protection against corrosion. As a result, corrosion of iron started to prevail, although not all the zinc was consumed [9,10]. Iron was oxidized to iron ions at the anodic sites, while O_2 was reduced to OH^-. Due to concentration gradient, the Fe^{2+} and OH^- diffused through the pores of the coating film and reacted with each other and formed ferrous hydroxide ($Fe(OH)_2$). After complex oxidization and dehydration reactions in this aerobic environment, these ferrous hydroxides were finally converted into iron oxide-hydroxides and iron oxide (α-FeOOH, β-FeOOH, γ-FeOOH, γ-Fe_2O_3, and a few amount of Fe_3O_4).

However, for the coatings with Fe_xP (Fig. 9b), the lamellar shaped electrically conductive Fe_xP could not only relieve the attack of corrosive species by increasing the tortuous paths of diffusion, but also maintain sufficient electrical connections among zinc particles and the substrate on a decreased zinc content. The Fe_xP activated zinc to corrode quickly at the beginning of immersion together with the electrolyte ingress, generating more corrosion products to block the channels. As a result, the enhanced barrier effect also led to the formation of more O_2 depleted corrosion products (Fig. 8) such as compact magnetite (Fe_3O_4) (Fig. 7) [59], which would additionally inhibit corrosion progression (Fig. 6). In the areas away from mechanical damage, the cathodic protection of connected zinc and improved barrier effect were able to inhibit the formation and progression of localized corrosion.

Conclusions

In summary, this is the first report incorporating economical iron phosphide powder into environmentally friendly zinc-rich polyester powder coatings for reducing zinc content. We investigated anti-corrosive performance of the obtained coating panels by OCP, EIS measurements and neutral salt spray tests, and analyzed the corrosion products using OM, XRD, Raman and SEM/EDS. It was found that iron phosphide was able to establish cathodic protection at a zinc content as low as 45 wt%. The Zn65P10 replaced 10 wt% zinc out of the 75 wt% zinc. A 40 μm zinc-rich polyester powder coating can almost maintain the pristine cathodic protection period (86 days). 10 wt% Fe_xP significantly decreased the average corrosion creepage from 1.78 mm to 1.42 mm after 2500 h of salt spray tests, diminished the localized corrosion. In addition, the Zn65P10 demonstrated a high impedance modulus of 6.4 MΩ cm^2 at the 0.01 Hz after 103 days of immersion. The superior corrosion resistance of iron phosphide containing coating films can be attributed to four reasons: conductive nature, inert chemistry, activation function, and barrier effects of the lamellar iron phosphide. This study would not only contribute to the development of environmentally friendly low zinc-content coatings for heavy duty applications, but also inspire the exploration of non-carbon-based conductive additives without zinc promotion effects and their utilization in corrosion protection.

CRediT authorship contribution statement

Jinbao Huang: Conceptualization, Methodology, Investigation, Writing – original draft, Writing – review & editing. **Marshall Yang:** Methodology, Investigation, Validation, Writing – review & editing. **Wenhao Zhu:** Methodology, Investigation, Validation, Writing – review & editing. **Keyong Tang:** Methodology, Writing – review & editing. **Jian**

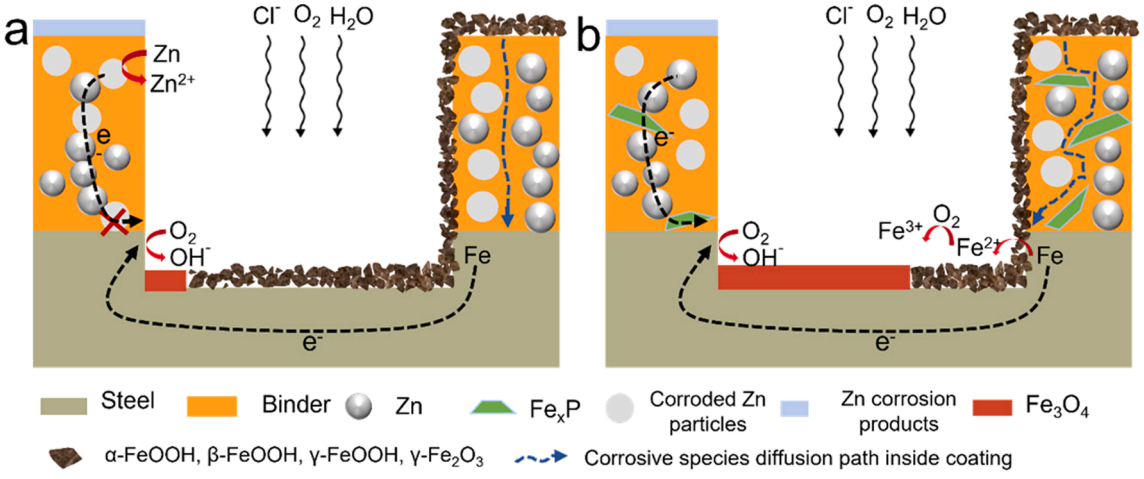

Fig. 9. Corrosion protection mechanisms for (a) zinc-rich powder coatings and (b) Fe_xP containing zinc-rich powder coatings.

Chen: Investigation, Validation, Writing – review & editing. **James Joseph Noël:** Investigation, Validation, Writing – review & editing. **Haiping Zhang:** Methodology, Writing – review & editing. **Liqin Wang:** Conceptualization, Methodology, Supervision, Writing – review & editing, Funding acquisition. **Hui Zhang:** Conceptualization, Methodology, Supervision, Writing – review & editing, Funding acquisition. **Jesse Zhu:** Conceptualization, Supervision, Writing – review & editing.

Declaration of Competing Interest

The authors declare that they have no known competing financial interests or personal relationships that could have appeared to influence the work reported in this paper.

Acknowledgement

This work was supported by the Key Basic Research Project (No. J2019-IV-0004-0071), the Natural Sciences and Engineering Research Council of Canada (Grant RGPIN-2018-06256 and RGPIN-2018-06672), China Scholarship Council (CSC) (No. 201707040063), Zhengzhou University, as well as the Department of Chemistry at Western University.

Appendix A. Supplementary data

Supplementary data to this article can be found online at https://doi.org/10.1016/j.jiec.2023.12.035.

References

[1] J.R. Vilche, E.C. Bucharsky, C.A. Giúdice, Application of EIS and SEM to evaluate the influence of pigment shape and content in ZRP formulations on the corrosion prevention of naval steel, Corros Sci. 44 (2002) 1287–1309, https://doi.org/10.1016/S0010-938X(01)00144-5.
[2] P.A. Sørensen, S. Kiil, K. Dam-Johansen, C.E. Weinell, Anticorrosive coatings: A review, J Coat Technol Res. 6 (2009) 135–176, https://doi.org/10.1007/s11998-008-9144-2.
[3] C.M. Abreu, M. Izquierdo, M. Keddam, X.R. Nóvoa, H. Takenouti, Electrochemical behaviour of zinc-rich epoxy paints in 3% NaCl solution, Electrochim Acta. 41 (1996) 2405–2415, https://doi.org/10.1016/0013-4686(96)00021-7.
[4] A. Kalendová, Effects of particle sizes and shapes of zinc metal on the properties of anticorrosive coatings, Prog Org Coat. 46 (2003) 324–332, https://doi.org/10.1016/S0300-9440(03)00022-5.
[5] J. Ruf, Korrosion-schutz durch lacke und pigmente, Colomb (1972).
[6] S. Feliu, R. Barajas, J.D. Bastidas, M. Morcillo, Mechanism of cathodic protection of zinc-rich points by electrochemical impedance spectroscopy. I: Galvanic stage, JCT, Journal of Coatings Technology. 61 (1989).
[7] C.H. Hare, Trouble with zinc-rich primers, Part I: non-topcoated systems, Journal of Protective Coatings & Linings. 15 (1998).
[8] D. Xie, The development of zinc-rich paints, Journal of Chinese Society for Corrosion and Protection. 24 (2009) 314–320.
[9] C.E. Weinell, S.N. Rasmussen, Advancement in zinc rich epoxy primers for corrosion protection, NACE - International Corrosion Conference Series. (2007) 070071–0700713.
[10] H. Marchebois, C. Savall, J. Bernard, S. Touzain, Electrochemical behavior of zinc-rich powder coatings in artificial sea water, Electrochim Acta. 49 (2004) 2945–2954, https://doi.org/10.1016/j.electacta.2004.01.053.
[11] S. Felui, J.M. Bastidas, M. Morcillo, S. Feliu, Effect of the Di-iron phosphide conductive extender on the protective mechanisms of zinc-rich coatings, Journal of Coatings Technology. 63 (1991) 67–72.
[12] S. Feliu, M. Morcillo, J.M. Bastidas, S. Feliu, Zinc reactivity in zinc-rich coatings co-pigmented with di-iron phosphide, Journal of Coatings Technology. 63 (1991) 31–34.
[13] S. Feliu, M. Morcillo, S. Feliu, Deterioration of Cathodic Protection Action of Zinc-Rich Paint Coatings in Atmospheric Exposure, Corrosion. 57 (7) (2001) 591–597.
[14] N.C. Fawcett, C.E. Stearns, B.G. Bufkin, Effect of zinc oxidation on the conductivity and performance of di-iron phosphide augmented zinc-rich primers, JCT, Journal of Coatings Technology. 56 (1984).
[15] B. Ramezanzadeh, S.Y. Arman, M. Mehdipour, Anticorrosion properties of an epoxy zinc-rich composite coating reinforced with zinc, aluminum, and iron oxide pigments, J Coat Technol Res. 11 (2014) 727–737, https://doi.org/10.1007/s11998-014-9580-0.
[16] H. Marchebois, S. Joiret, C. Savall, J. Bernard, S. Touzain, Characterization of zinc-rich powder coatings by EIS and Raman spectroscopy, Surf Coat Technol. 157 (2002) 151–161, https://doi.org/10.1016/S0257-8972(02)00147-0.
[17] A. Meroufel, S. Touzain, EIS characterisation of new zinc-rich powder coatings, Prog Org Coat. 59 (2007) 197–205, https://doi.org/10.1016/j.porgcoat.2006.09.005.
[18] S. Teng, Y. Gao, F. Cao, D. Kong, X. Zheng, X. Ma, L. Zhi, Zinc-reduced graphene oxide for enhanced corrosion protection of zinc-rich epoxy coatings, Prog Org Coat. 123 (2018) 185–189, https://doi.org/10.1016/j.porgcoat.2018.07.012.
[19] Z. Song, B. Qian, Effect of graphene on the electrochemical protection of zinc-rich coatings, Materials and Corrosion. 69 (2018) 1854–1860, https://doi.org/10.1002/maco.201810312.
[20] H. Hayatdavoudi, M. Rahsepar, A mechanistic study of the enhanced cathodic protection performance of graphene-reinforced zinc rich nanocomposite coating for corrosion protection of carbon steel substrate, J Alloys Compd. 727 (2017) 1148–1156, https://doi.org/10.1016/j.jallcom.2017.08.250.
[21] S.M. Park, M.Y. Shon, Effects of multi-walled carbon nano tubes on corrosion protection of zinc rich epoxy resin coating, Journal of Industrial and Engineering Chemistry. 21 (2015) 1258–1264, https://doi.org/10.1016/j.jiec.2014.05.042.
[22] T. Ge, W. Zhao, X. Wu, X. Lan, Y. Zhang, Y. Qiang, Y. He, Incorporation of electroconductive carbon fibers to achieve enhanced anti-corrosion performance of zinc rich coatings, J Colloid Interface Sci. 567 (2020) 113–125.
[23] K. Yang, Y. Duan, G. Liu, G. Ma, H. Fu, X. Chen, M. Wang, G. Zhu, W. Yang, Y. Shen, Smart ZnS@C filler for super-anticorrosive self-healing zinc-rich epoxy coating, Nano Res. 15 (2022) 4756–4764, https://doi.org/10.1007/s12274-022-4161-5.
[24] C.E.W. Qi, Chunping, Kim Dam-Johansen, H.W. Bi, Huichao, Enhanced anticorrosion performance of zinc rich epoxy coatings modified with stainless steel flakes, Prog Org Coat. 163 (2022). https://www.sciencedirect.com/science/article/pii/S0300944021004872?via%3Dihub.
[25] Y. Bai, X. Jin, J. Xie, X. Lv, T. Guo, L.i. Zhang, J. Zhu, Y. Shao, H. Zhang, H. Zhang, B. Yuan, A. Yin, J. Nie, F. Cao, Z. Xu, Fabrication of a Conductive Additive for the Anticorrosion Enhancement of Zinc-Rich Epoxy Coatings, Coatings. 12 (10) (2022) 1406.
[26] C. Qi, C.E. Weinell, K. Dam-Johansen, H. Wu, Assessment of Anticorrosion Performance of Zinc-Rich Epoxy Coatings Added with Zinc Fibers for Corrosion Protection of Steel, ACS Omega. (2022), https://doi.org/10.1021/ACSOMEGA.2C03738/ASSET/IMAGES/LARGE/AO2C03738_0014.JPEG.
[27] K. Schaefer, A. Miszczyk, Improvement of electrochemical action of zinc-rich paints by addition of nanoparticulate zinc, Corros Sci. 66 (2013) 380–391, https://doi.org/10.1016/j.corsci.2012.10.004.
[28] N. Arianpouya, M. Shishesaz, M. Arianpouya, M. Nematollahi, Evaluation of synergistic effect of nanozinc/nanoclay additives on the corrosion performance of zinc-rich polyurethane nanocomposite coatings using electrochemical properties and salt spray testing, Surf Coat Technol. 216 (2013) 199–206, https://doi.org/10.1016/j.surfcoat.2012.11.036.
[29] C.H. Hare, S.J. Wright, Anti-corrosive primers based on zinc flack, (1982).
[30] S. Touzain, Accelerated aging of zinc-rich powder coatings containing different conductive pigments, Powder Coating Pigments. (2009) 1–6.
[31] A. Meroufel, C. Deslouis, S. Touzain, Electrochemical and anticorrosion performances of zinc-rich and polyaniline powder coatings, Electrochim Acta. 53 (2008) 2331–2338, https://doi.org/10.1016/j.electacta.2007.09.056.
[32] L. Shen, W. Zhao, K. Wang, J. Xu, GO-Ti3C2 two-dimensional heterojunction nanomaterial for anticorrosion enhancement of epoxy zinc-rich coatings, J Hazard Mater. 417 (2021) 126048, https://doi.org/10.1016/J.JHAZMAT.2021.126048.
[33] F.T. Shirehjini, I. Danaee, H. Eskandari, S. Nikmanesh, D. Zarei, Improvement of the sacrificial behavior of zinc in scratches of zinc-rich polymer coatings by incorporating clay nanosheets, Materialpruefung/materials Testing. 59 (2017) 682–688, https://doi.org/10.3139/120.111057.
[34] M. Zhang, H. Wang, T. Nie, J. Bai, F. Zhao, S. Ma, Enhancement of barrier and anti-corrosive performance of zinc-rich epoxy coatings using nano-silica/graphene oxide hybrid, Corrosion Reviews. 38 (2020) 497–513.
[35] W. Sun, L. Wang, T. Wu, M. Wang, Z. Yang, Y. Pan, G. Liu, Inhibiting the Corrosion-Promotion Activity of Graphene, Chemistry of Materials. 27 (2015) 2367–2373, https://doi.org/10.1021/cm5043099.
[36] J. Ding, H. Zhao, H. Yu, Superior and durable graphene-based composite coatings by bioinspired interfaces and alignment, Compos Sci Technol. 214 (2021) 108967.
[37] M. Schriver, W. Regan, W.J. Gannett, A.M. Zaniewski, M.F. Crommie, A. Zettl, Graphene as a Long-Term Metal Oxidation Barrier: Worse Than Nothing, Graphene as a Long-Term Metal Oxidation Barrier: Worse than Nothing 7 (7) (2013) 5763–5768.
[38] M. Cai, H. Yan, Y. Li, W. Li, X. Fan, M. Zhu, Elucidating the electrochemical mechanism for enhanced corrosion of Ti3C2Tx-coated mild steel, Surf Topogr. 9 (3) (2021) 035033.
[39] E. Langer, M. Zubielewicz, H. Kuczyńska, A. Królikowska, L. Komorowski, Anticorrosive effectiveness of coatings with reduced content of Zn pigments in comparison with zinc-rich primers, Corrosion Engineering Science and Technology. 54 (2019) 627–635, https://doi.org/10.1080/1478422X.2019.1652428.
[40] D.M. Xie, K. Huang, X. Feng, Y.G. Wang, Improving the performance of zinc-rich coatings using conductive pigments and silane, Corrosion Engineering Science and Technology. 55 (2020) 539–549, https://doi.org/10.1080/1478422X.2020.1759484.
[41] M.S. Yang, J. Huang, J.J. Noël, J. Chen, I. Barker, J.D. Henderson, H. Zhang, H. Zhang, J. Zhu, A Mechanistic Study on the Anti-Corrosive Performance of Zinc-Rich Polyester/TGIC Powder Coatings, Processes. 10 (2022) 1853, https://doi.org/10.3390/PR10091853/S1.
[42] J. Huang, M. Yang, W. Zhu, K. Tang, H. Zhang, J. Chen, J.J. Noël, I. Barker, H. Zhang, J. Zhu, Extrusion-free fabrication of zinc-rich powder coatings: Press

bonding, Chemical Engineering Journal. 442 (2022) 135925, https://doi.org/10.1016/J.CEJ.2022.135925.
[43] N.S. RP-01-69, Control of External Corrosion on Underground or Submerged Metallic Piping Systems, Mater. Prot. 8 (1969) 1.
[44] J.R. Scully, Electrochemical Impedance of Organic-Coated Steel: Correlation of Impedance Parameters with Long-Term Coating Deterioration, J Electrochem Soc. 136 (4) (1989) 979–990.
[45] H.P. Hack, J.R. Scully, Defect Area Determination of Organic Coated Steels in Seawater Using the Breakpoint Frequency Method, J Electrochem Soc. 138 (1) (1991) 33–40.
[46] J.M. McIntyre, H.Q. Pham, Electrochemical impedance spectroscopy; a tool for organic coatings optimizations, Prog Org Coat. 27 (1996) 201–207, https://doi.org/10.1016/0300-9440(95)00532-3.
[47] J.R. Scully, S.T. Hensley, Lifetime prediction for organic coatings on steel and a magnesium alloy using electrochemical impedance methods, Corrosion. 50 (1994) 705–716, https://doi.org/10.5006/1.3293547.
[48] S. Touzain, Q. Le Thu, G. Bonnet, Evaluation of thick organic coatings degradation in seawater using cathodic protection and thermally accelerated tests, in, Prog Org Coat, Elsevier (2005) 311–319, https://doi.org/10.1016/j.porgcoat.2004.09.007.
[49] H. Marchebois, S. Touzain, S. Joiret, J. Bernard, C. Savall, Zinc-rich powder coatings corrosion in sea water: Influence of conductive pigments, Prog Org Coat. 45 (2002) 415–421, https://doi.org/10.1016/S0300-9440(02)00145-5.
[50] J.H. Park, T.H. Yun, K.Y. Kim, Y.K. Song, J.M. Park, The improvement of anticorrosion properties of zinc-rich organic coating by incorporating surface-modified zinc particle, Prog Org Coat. 74 (2012) 25–35, https://doi.org/10.1016/j.porgcoat.2011.09.012.
[51] R. Ding, Y. Zheng, H. Yu, W. Li, X. Wang, T. Gui, Study of water permeation dynamics and anti-corrosion mechanism of graphene/zinc coatings, J Alloys Compd. 748 (2018) 481–495, https://doi.org/10.1016/j.jallcom.2018.03.160.
[52] S. Huang, G. Kong, B. Yang, S. Zhang, C. Che, Effects of graphene on the corrosion evolution of zinc particles in waterborne epoxy zinc-containing coatings, Prog Org Coat. 140 (2020) 105531, https://doi.org/10.1016/j.porgcoat.2019.105531.
[53] J. Ding, H. Zhao, B. Xu, X. Zhao, S. Su, H. Yu, Superanticorrosive Graphene Nanosheets through π Deposition of Boron Nitride Nanodots, ACS Sustainable Chemistry & Engineering. 7 (12) (2019) 10900–10911.
[54] J. Ding, H. Zhao, D. Ji, B. Xu, X. Zhao, Z. Wang, D. Wang, Q. Zhou, H. Yu, Achieving long-term anticorrosion: Via the inhibition of graphene's electrical activity, J Mater Chem A Mater. 7 (2019) 2864–2874, https://doi.org/10.1039/c8ta10337b.
[55] S.J. Oh, D.C. Cook, H.E. Townsend, Characterization of Iron Oxides Commonly Formed as Corrosion Products on Steel, Hyperfine Interactions 1998 112:1. 112 (1998) 59–66. https://doi.org/10.1023/A:1011076308501.
[56] R.A. Antunes, R.U. Ichikawa, L.G. Martinez, I. Costa, Characterization of corrosion products on carbon steel exposed to natural weathering and to accelerated corrosion tests, International Journal of Corrosion. 2014 (2014) 1–9.
[57] J.H. Ding, H.R. Zhao, Y. Zheng, X. Zhao, H. Bin Yu, A long-term anticorrsive coating through graphene passivation, Carbon N Y. 138 (2018) 197–206. https://doi.org/10.1016/j.carbon.2018.06.018.
[58] Y. Cubides, H. Castaneda, Corrosion protection mechanisms of carbon nanotube and zinc-rich epoxy primers on carbon steel in simulated concrete pore solutions in the presence of chloride ions, Corros Sci. 109 (2016) 145–161, https://doi.org/10.1016/j.corsci.2016.03.023.
[59] T. Standish, J. Chen, R. Jacklin, P. Jakupi, S. Ramamurthy, D. Zagidulin, P. Keech, D. Shoesmith, Corrosion of copper-coated steel high level nuclear waste containers under permanent disposal conditions, Electrochim Acta. 211 (2016) 331–342, https://doi.org/10.1016/J.ELECTACTA.2016.05.135.